Separation and Purification Technology 311 (2023) 123347

Contents lists available at ScienceDirect

Separation and Purification Technology

journal homepage: www.elsevier.com/locate/seppur

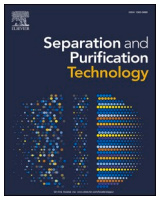

Effect of ZIF-7 doping content on H_2/CO_2 separation performance of 1,2-bis (triethoxysilyl)ethane-derived organosilica membranes

Yi Ren, Die He, Tong Wang, Hong Qi *

College of Chemical Engineering, Nanjing Tech University, Nanjing 211816, PR China

ARTICLE INFO

Keywords:
Zeolite imidazolate frameworks
Organosilica
Membranes
Hydrogen

ABSTRACT

Organosilica membranes with good hydrothermal stability are promising for pre-combustion capture, but the trade-off effect still constrains their gas separation performance. Herein, we prepared hybrid membranes by incorporating ZIF-7 nanoparticles into 1, 2-bis(triethoxysilyl)ethane (BTESE) networks to improve the H_2/CO_2 permselectivity by the intrinsic properties of nanoparticles. The effect of inorganic fillers was investigated by adjusting the doping content of ZIF-7 nanoparticles. We found that the H_2 permeance of hybrid membranes remained at $\sim 10^{-6}$ mol·m^{-2}·s^{-1}·Pa^{-1}, while the H_2/CO_2 permselectivity decreased with increasing nanoparticle doping content. The E-ZIF-7-0.4 hybrid membrane showed H_2 permeance of 1.2×10^{-6} mol·m^{-2}·s^{-1}·Pa^{-1} and H_2/CO_2 permselectivity of 21.7. Our results may offer valuable insights into preparing hybrid membranes with optimal nanoparticle doping content.

1. Introduction

Global warming and extreme weather events caused by greenhouse gas have generated growing concern. CO_2, one of the combustion byproducts of fossil fuels, accounts for the majority of greenhouse gas emissions [1]. Therefore, developing clean energy to reduce CO_2 emissions is an issue of considerable concern. Hydrogen is an environmentally-friendly energy carrier with high energy density [2]. It is primarily produced by water gas shift reactions [3]. Compared with conventional separation processes, membrane separation is a competitive technology for hydrogen purification owing to its low investment and easy operation processes [4–6]. Various high-performance materials have been explored, including polymers, inorganic materials, and mixed matrix membranes (MMMs) [7–9].

The microporous SiO_2 membranes have good chemical stability and mechanical strength, showing promise for gas separation. However, the employment of SiO_2 membranes is constrained by hydrothermal stability. The chemical structures of SiO_2 membranes become unstable under water vapor, resulting in a significant loss of gas permeability [10,11]. It is feasible to improve the hydrothermal stability of SiO_2 membranes by introducing organic groups into silica networks. Organosilica membranes prepared from organoalkoxysilanes, such as BTESE, have been rapidly developed in recent years. BTESE-derived membranes are stable under hydrothermal conditions owing to their intrinsic hydrophobic properties. Tsuru et al. [12] first prepared BTESE membranes with excellent H_2 permeance and hydrophobic properties. However, the large pore size induced by Si–CH_2–CH_2–Si bonds in the BTESE structure makes it challenging to separate H_2 and CO_2 [13]. Some strategies have been adopted to optimize the gas separation capabilities of BTESE membranes, including copolymerization of precursors [14,15], optimization of sols preparation [16,17], optimization of calcination parameters [18], metals and metal–organic frameworks (MOFs) doping [19,20].

MOFs are novel hybrid materials composed of organic linkers and metal ions with merits such as regular pore channels and tunable structures [21]. Zeolite imidazolate frameworks (ZIFs), an essential MOFs branch, have made significant advancements due to tunable pore size and good stability [22]. However, industrial-scale fabrication of ZIFs membranes is still challenging [23,24]. MMMs overcome this problem by incorporating ZIFs nanoparticles into polymer matrix, combining the easy processing of polymers and the intrinsic properties of ZIFs to prepare novel hybrid materials. Shafiq et al. [25] first mixed ZIF-95 nanoparticles with polysulfone (PSF) at different weight percentages to prepare MMMs. Compared with pure PSF membranes, the H_2 permeance and the H_2/CO_2 permselectivity of the optimal loading MMMs (24 wt% ZIF-95 loading) increased by 80.2 % and 8 %, respectively. Wang et al. [26] reported ZIF-7-NH_2/PIM-1 MMMs with enhanced selectivity for biogas purification. The strong interactions

* Corresponding author.
E-mail address: hqi@njtech.edu.cn (H. Qi).

https://doi.org/10.1016/j.seppur.2023.123347
Received 22 November 2022; Received in revised form 20 January 2023; Accepted 31 January 2023
Available online 3 February 2023

Table 1
Parameters of homemade tubular γ-Al_2O_3/α-Al_2O_3 supports.

Parameter	Value
Average pore size (nm)	5
Inner diameter (mm)	8
Outer diameter (mm)	12
Length (mm)	50

Table 2
The Molar amount of each component in the synthesis of E-ZIF-7-*x* hybrid sols.

sols	ZIF-7 nanoparticles (mmol)	BTESE (mmol)	EtOH (mol)
E-ZIF-7-0.2	0.85	4.24	0.72
E-ZIF-7-0.4	1.70	4.24	0.72
E-ZIF-7-0.6	2.54	4.24	0.72
E-ZIF-7-0.8	3.39	4.24	0.72
E-ZIF-7-1	4.24	4.24	0.72

between nanoparticles and polymer improved the efficiency of biogas purification of the MMMs. The corresponding membranes had CO_2 permeance of 2.1 × 10^{-8} mol·m^{-2}·s^{-1}·Pa^{-1} and CO_2/CH_4 permselectivity of 90.4. Yang et al. [27] prepared MMMs by introducing ZIF-7 nanoparticles to the poly 2,2′-(*p*-oxydiphenyl)-5,5′-bibenzimidazole (OPBI) networks. The OPBI membrane with optimal nanoparticle doping content exhibited H_2/CO_2 permselectivity of 13.5 measured at 180 ℃. Yoon et al. [28] prepared membranes for post-combustion capture by mixing ZIF-7 nanoparticles with the Pebax-2533 matrix. The ZIF-7/Pebax-2533 membrane containing 35 wt% ZIF-7 nanoparticles had high CO_2 permeance (1.0 × 10^{-6} mol·m^{-2}·s^{-1}·Pa^{-1}) and CO_2/N_2 permselectivity (50.4). Hence, the optimal doping content of ZIFs nanoparticles provides additional gas permeation channels to overcome the trade-off effect. In contrast, overdoping may cause severe incompatibility between nanoparticles and polymer matrix, resulting in poor gas permselectivity.

As mentioned above, the doping content of nanoparticles can significantly influence the gas separation performance of MMMs. Nevertheless, few studies on MOF-doped organosilica membranes have been conducted. Kong et al. [29] first reported MOF-doped BTESE membranes on tubular ceramic supports with good gas separation performance. MOF/BTESE hybrid membranes have advantages of BTESE, such as good hydrothermal stability, high affinity with high affinity to inorganic material supports, and unique properties of MOFs, like regular pore structure and tunable pore size. These merits can significantly enhance the permeance and permselectivity of MOF/organosilica hybrid materials. In their study, ZIF-8 nanoparticles were selected as inorganic fillers and subsequently incorporated into BTESE networks. The ZIF-8/BTESE sols with different weight ratios of ZIF-8 to BTESE (W*r* = 1:2, 1:1, 2:1) were prepared to fabricate the ZIF-8/BTESE hybrid membranes. The H_2 permeance of the ZIF-8/BTESE hybrid membranes increased from ~7.0 × 10^{-7} to ~1.1 × 10^{-6} mol·m^{-2}·s^{-1}·Pa^{-1} with the increase of ZIF-8 doping content. However, the H_2/CO_2 permselectivity of the ZIF-8/BTESE hybrid membranes was lower than 5, which may be caused by the larger pore size of ZIF-8 (0.33 nm). ZIF-7 is an essential member of the ZIFs family that has received much attention. The organic and inorganic components in the structures of ZIF-7 and BTESE allow for good compatibility between ZIF-7 and BTESE. In addition, ZIF-7 has an appropriate window size of ~0.3 nm [27], which is more suitable for H_2/CO_2 separation than ZIF-8.

In this work, nanoparticles were introduced into organosilica networks at various molar ratios of MOF to organosilica. The hybrid membranes were fabricated by coating hybrid sols onto the tubular γ-Al_2O_3/α-Al_2O_3 supports, followed by calcination under nitrogen. The nanoparticles were confirmed to be introduced into BTESE networks by various characterizations. The doping content of nanoparticles on the gas separation performance concerning the MOF/organosilica hybrid membranes was preliminarily investigated. ZIF-7 nanoparticles in the BTESE networks provide not only additional gas permeation channels within the hybrid membranes but also molecular-sieving pores endowed by the intrinsic properties of nanoparticles. The E-ZIF-7-0.4 membrane had good H_2/CO_2 separation performance owing to the synergetic effects of nanoparticles and organosilica networks.

2. Materials and methods

2.1. Materials

1, 2-bis(triethoxysilyl)ethane (BTESE, 97 %, Gelest), zinc nitrate hexahydrate (Zn $(NO_3)_2$·$6H_2O$, 99.8 %, Sinopharm), benzimidazole (BzIM, 98 %, Aladdin), methanol (MeOH, 99.5 %, Yasheng), *N, N*-dimethylformamide (DMF, 99.5 %, Yasheng), and anhydrous ethanol (EtOH, 99.5 %, Yasheng) were used without further purification. The concentrated hydrochloric acid (HCl, 36 wt%, Lingfeng) was diluted to 1 mol·L^{-1} for further use. The parameters of homemade tubular γ-Al_2O_3/α-Al_2O_3 supports are listed in Table 1.

2.2. Preparation of nanoparticles

ZIF-7 was synthesized using the method described by Li et al. [30]. Specifically, BzIM (5 mmol) and zinc nitrate hexahydrate (5 mmol) were dissolved in MeOH (50 mL) and DMF (50 mL), respectively. The Zn^{2+} salt solution was rapidly added to the BzIM solution and was reacted with stirring at 25 ℃ for 6 h. The obtained products were followed by 5 min centrifugal treatment (10000 rpm) and purified with fresh MeOH. Finally, ZIF-7 nanoparticles were dried at 60 ℃ overnight.

2.3. Preparation of BTESE sols

The organosilica sols were synthesized as reported in our previous work [20]. BTESE (5 mL) and EtOH (10 mL) were blended in the ice bath. The solution containing EtOH (5 mL), deionized water (5 mL), and HCl (0.5 mL) was introduced into the BTESE/EtOH mixture and stirred at 60 ℃ for 90 min.

2.4. Preparation of hybrid sols and membranes

The following procedures were performed to prepare MOF/organosilica hybrid sols. First, requisite masses of ZIF-7 nanoparticles were dissolved in EtOH (42 mL) via sonication for 15 min. Then, BTESE sols (8 mL) were added to the ZIF-7/EtOH mixture with further sonication for 10 min. The obtained ZIF-7/BTESE sols were then adjusted to pH = 3 with HCl. The resulting sols, powders, and hybrid membranes were marked as E-ZIF-7-*x* (*x* = 0.2, 0.4, 0.6, 0.8, and 1) based on the molar ratios of nanoparticles to organosilica. Table 2 displays the molar amount of each component in the synthesis of E-ZIF-7-*x* hybrid sols.

The E-ZIF-7-*x* hybrid membranes were fabricated by applying hybrid sols to the tubular γ-Al_2O_3/α-Al_2O_3 supports using the dip-coating method. The freshly prepared E-ZIF-7-*x* hybrid membranes were treated in a temperature-humidity chamber at constant temperature and humidity for 60 min and then calcined at 400 °C for 180 min under nitrogen. The E-ZIF-7-*x* powders were obtained by drying hybrid sols and then calcined using the same calcination processes for preparing hybrid membranes.

2.5. Characterization

The size of the hybrid sols was measured by dynamic light scattering (DLS, ZS 90). X-ray diffraction (XRD, MiniFlex 600), X-ray photoelectron spectroscopy (XPS, ESCALAB 250), and Fourier transform infrared spectrometer (FT-IR, Nicolet 8700) were performed to investigate the

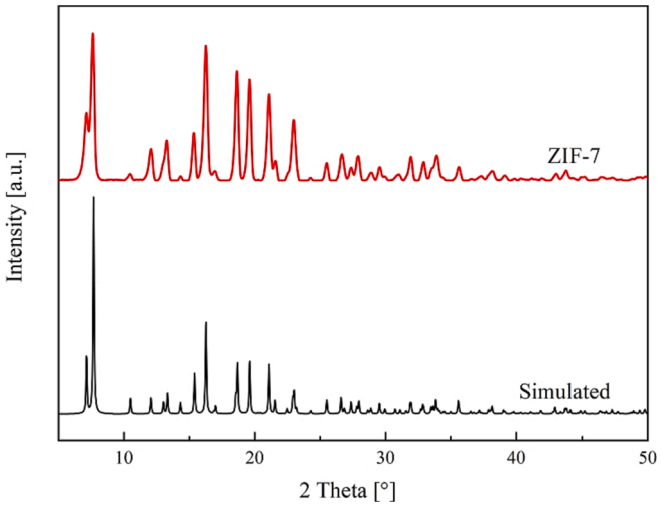

Fig. 1. XRD patterns of MOF nanoparticles.

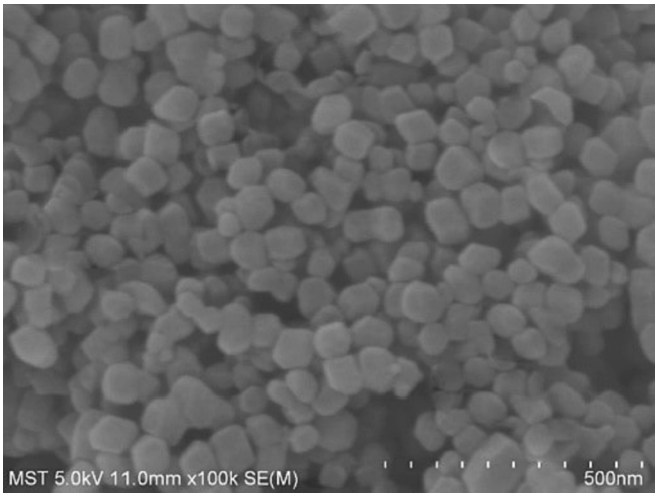

Fig. 2. SEM image of MOF nanoparticles.

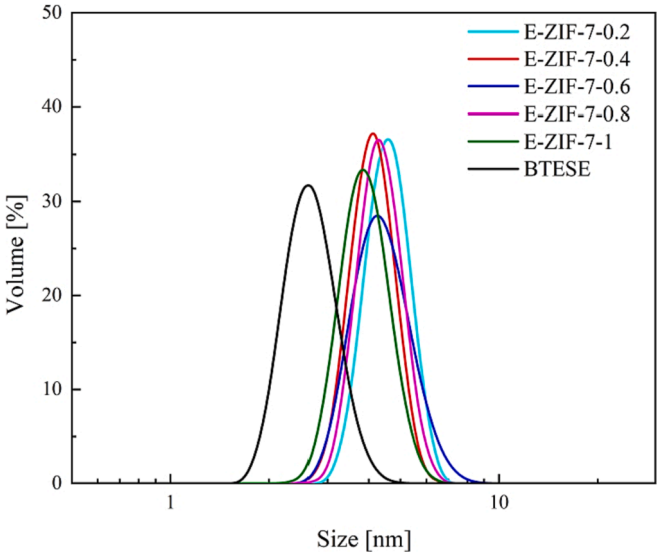

Fig. 3. Size distribution of sols.

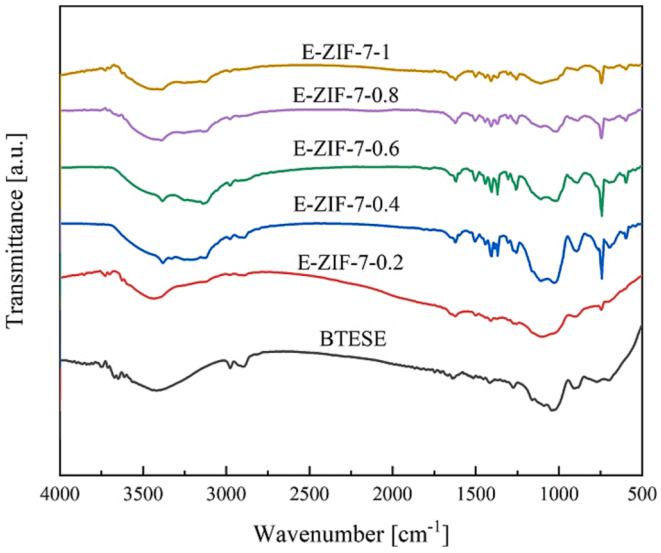

Fig. 4. FT-IR spectra of organosilica and MOF/organosilica powders.

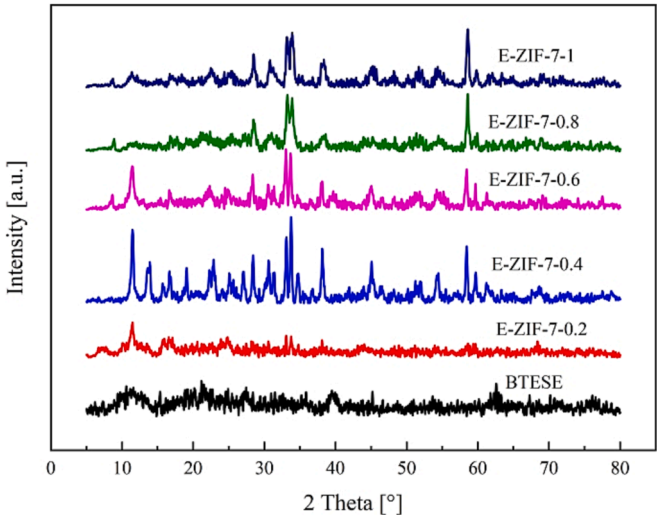

Fig. 5. XRD patterns of organosilica and MOF/organosilica powders.

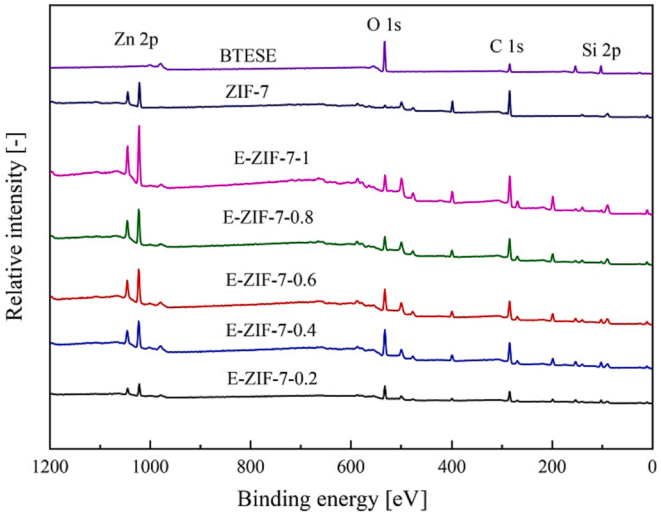

Fig. 6. XPS spectra of organosilica and MOF/organosilica powders.

Table 3
Elemental content of organosilica and MOF/organosilica powders.

Samples	Elemental content / %			
	Si	C	O	Zn
E-ZIF-7-0.2	14.6	51.8	27	6.6
E-ZIF-7-0.4	11.6	54.4	24.4	9.6
E-ZIF-7-0.6	11.4	53.4	24.8	10.4
E-ZIF-7-0.8	6.6	64.3	17.7	11.4
E-ZIF-7-1	5.2	67.3	15	12.5
BTESE	23.5	30.7	45.8	0

crystal structures, the elemental content, and the chemical structures of ZIF-7 and MOF/organosilica powders, respectively. The CO_2 adsorption properties of the E-ZIF-7-0.4, BTESE, and ZIF-7 powders were measured at 298 K by Physical Adsorbent (ASAP 2000) and were vacuum pre-treated at 473 K overnight. Scanning electron microscope (SEM, S 4800) and Transmission electron microscope (TEM, JEM 200CX) were used to analyze the morphology of MOF/organosilica powders.

2.6. Membranes performance evaluation

Single-gas permeation performances of the E-ZIF-7-*x* hybrid membranes were evaluated at 200 ℃ with a bubble flow meter [14], and the trans-membrane pressure in the single gas permeation test was 0.3 MPa.

The single-gas permeances (F_i) are calculated using Eq. (1):

$$F_i = \frac{M_i}{S\Delta P} \tag{1}$$

where M_i is the molar flow rate of gas *i*, *S* is the effective membrane area, and ΔP is the trans-membrane pressure drop.

The permselectivity (α) is calculated using Eq. (2):

$$\alpha = \frac{F_i}{F_j} \tag{2}$$

where F_i and F_j are the permeance of gases.

3. Results and discussion

3.1. Characterization of MOFs

All of the XRD patterns of as-synthesized ZIF-7 nanoparticles shown in Fig. 1 resemble those of simulated, suggesting successful nanoparticle preparation. Fig. 2 shows that the particle size of the as-synthesized nanoparticles is approximately 60 nm.

3.2. Size distribution of sols

It is evident from Fig. 3 that the mean size of the organosilica sols is approximately 4 nm. Notably, the E-ZIF-7-*x* hybrid sols exhibit size distribution from 3 to 10 nm, indicating that the size of hybrid sols was not significantly affected by ZIF-7 nanoparticles doping content. The average particle size distribution of the E-ZIF-7-*x* hybrid sols was smaller

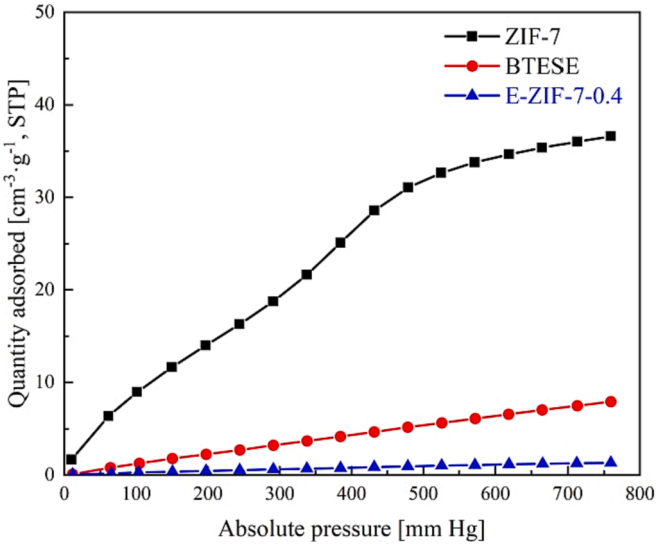

Fig. 8. CO_2 adsorption isotherms of BTESE, ZIF-7, and E-ZIF-7-0.4 powders.

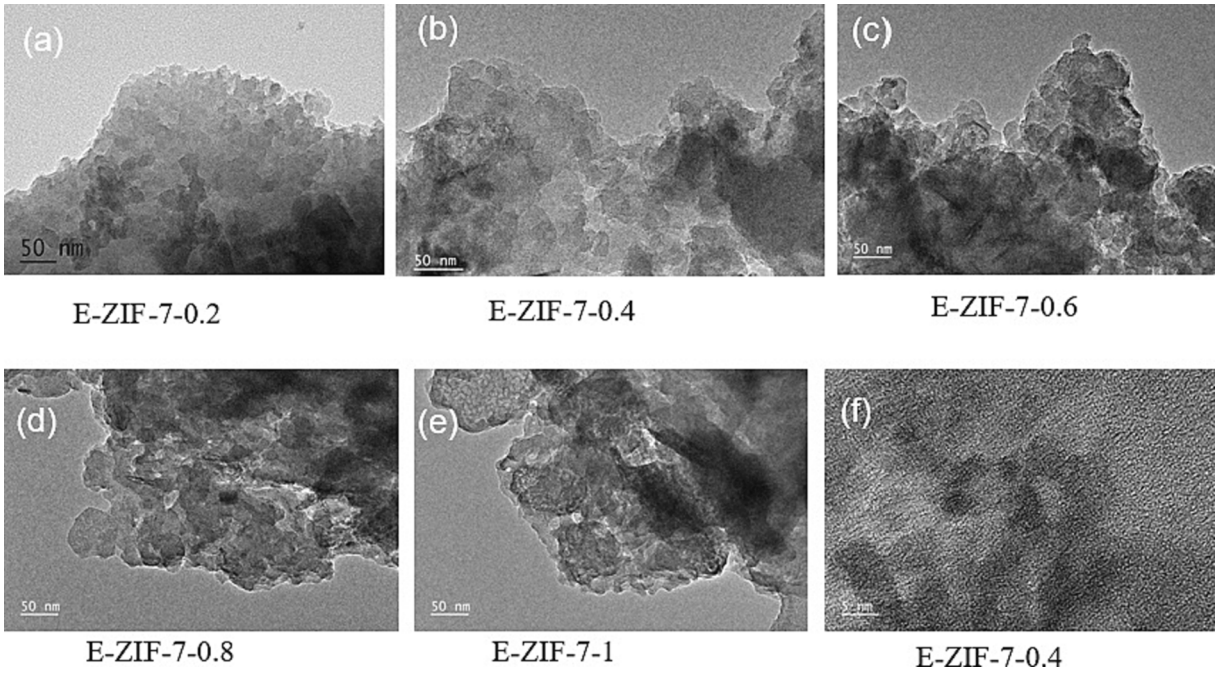

Fig. 7. TEM images of E-ZIF-7-*x* powders (a) $x = 0.2$, (b, f) $x = 0.4$, (c) $x = 0.6$, (d) $x = 0.8$, and (e) $x = 1$.

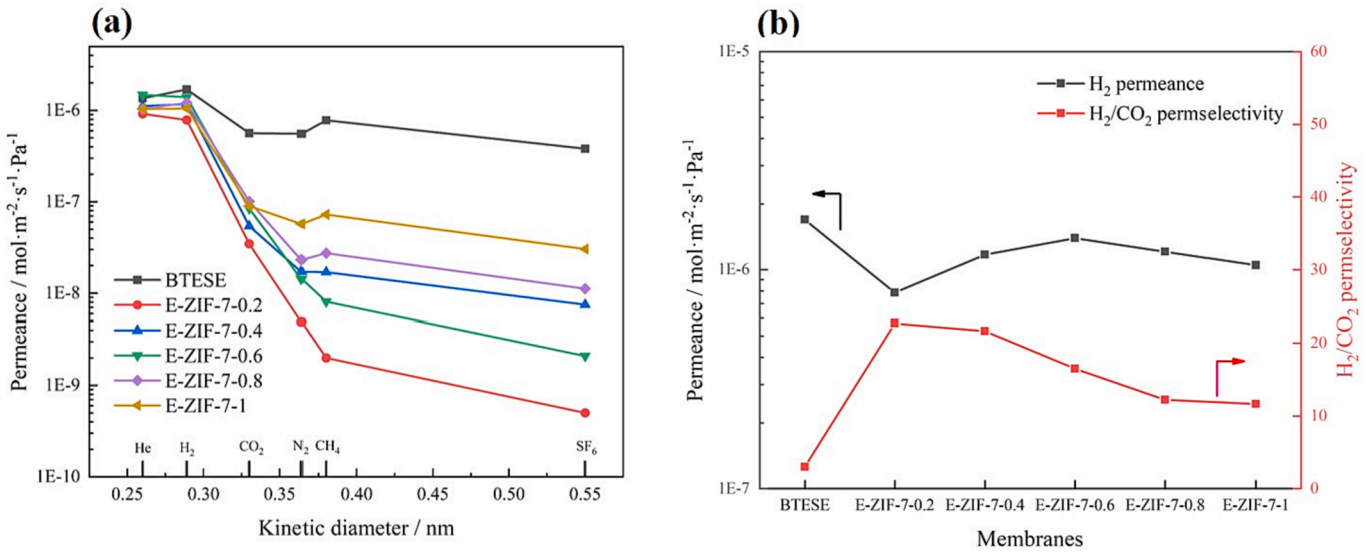

Fig. 9. (a) Gas permeances and (b) H_2/CO_2 separation performance of BTESE and E-ZIF-7-*x* hybrid membranes measured at 200 ℃.

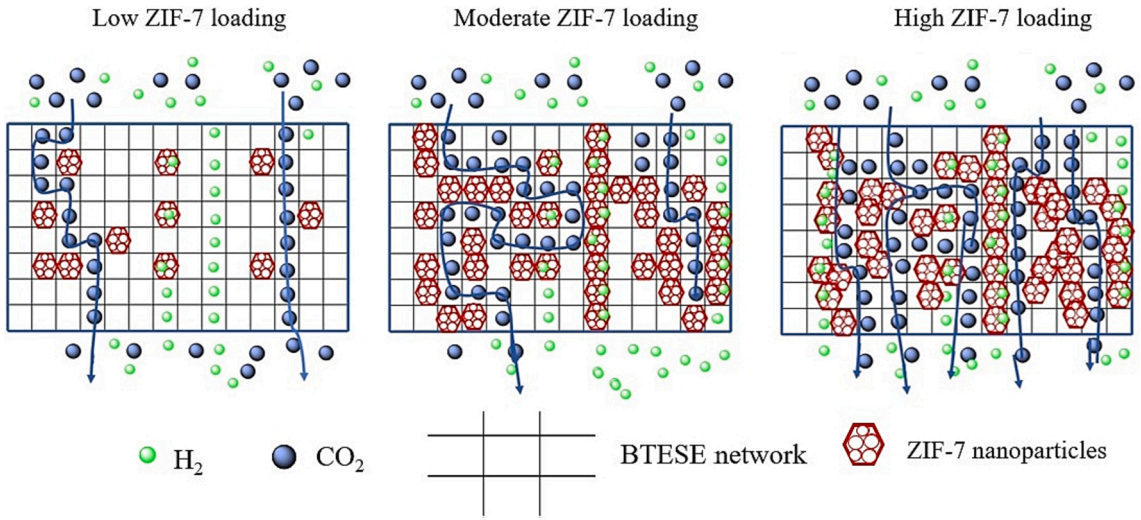

Fig. 10. Schematic diagram of gas separation performance of E-ZIF-7-*x* hybrid membranes.

than that of ZIF-7, which could be attributed to the ultrasonic treatment. The decreased average particle size of the E-ZIF-7-*x* hybrid sols was observed after ultrasonic treatment, while the crystal structure of ZIF-7 was maintained, as evidenced by XRD patterns and FTIR spectra. Moreover, the average size of hybrid sols is comparable to the average pore size of the γ-Al_2O_3/α-Al_2O_3 supports, which facilitates the preparation of the separation layer.

3.3. Chemical properties of powders

The FT-IR spectra of the organosilica and MOF/organosilica powders are provided in Fig. 4. The peaks at ~3450 and ~1630 cm^{-1} for all powders were from the stretching vibrations of the silanol bonds [31]. The peaks at ~1030 cm^{-1} were from the asymmetric stretching vibrations of the siloxane bonds [32]. In contrast to organosilica powders, new chemical bonds can be observed at ~1506 and ~743 cm^{-1} in E-ZIF-7-*x* powders, which can be attributed to the C═C [33] and C—H [34] bonds in the ZIF-7 structures, respectively.

Fig. 5 shows the XRD characterization of the organosilica and MOF/organosilica powders. Notably, no typical diffraction peaks can be observed in the BTESE powders, suggesting the amorphous structure of BTESE [35]. The characteristic peaks of nanoparticles were detected in the E-ZIF-7-*x* powders, suggesting that the crystal structures of nanoparticles were preserved when incorporated into BTESE networks. The shift of the peaks and the variation of the peak intensity were observed in the XRD patterns. When MOF nanoparticles are incorporated into the polymer network, the XRD patterns should be determined by both MOF nanoparticles and the polymer, which may cause the shift of the peaks and the peak intensity variation [26,36].

The elemental composition of organosilica, ZIF-7, and MOF/organosilica powders could be further identified by the XPS characterization. As displayed in Fig. 6, the elements C, O, and Si were detected in the organosilica powders, while Zn and C elements were seen in the nanoparticle powders. When nanoparticles were incorporated into organosilica networks, Si and Zn elements could be simultaneously detected in E-ZIF-7-*x* powders. Notably, the Zn 2p characteristic peak intensity in the corresponding E-ZIF-7-*x* powders increased with the ZIF-7 doping content. Table 3 summarizes the elemental content of organosilica and MOF/organosilica hybrid powders. The Zn/Si ratios in the E-ZIF-*x* powders increased from 0.45 to 2.4, due mainly to the increase of ZIF-7 doping content. The molar ratios of ZIF-7 and BTESE in the E-ZIF-*x* powders calculated using XPS were 0.23, 0.41, 0.46, 0.87, and 1.2,

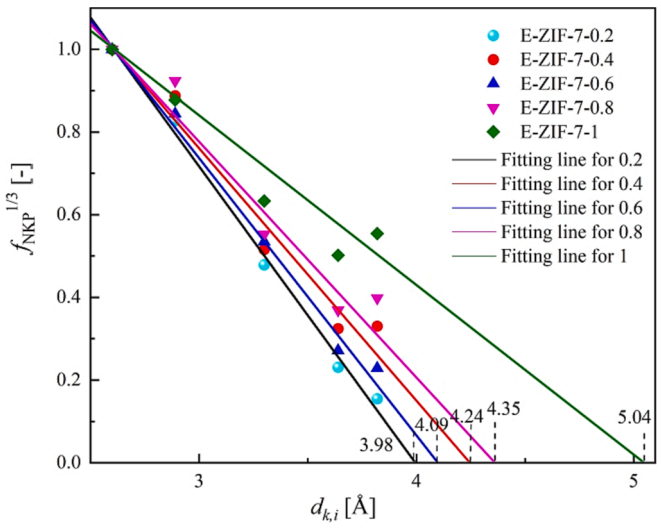

Fig. 11. NKP plot as a function of molecule size of E-ZIF-7-*x* hybrid membranes.

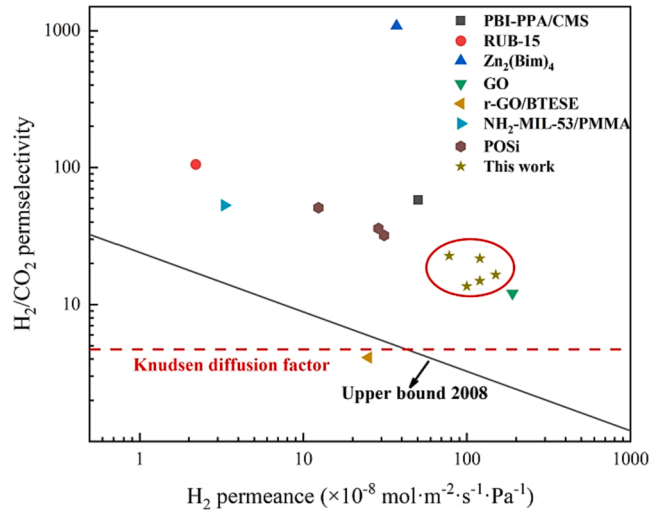

Fig. 12. Comparison of H_2/CO_2 separation performance of hybrid membranes with reported membranes (The upper bound 2008 line was drawn by assuming the membranes thickness of 100 nm) [42–48].

respectively. There are some deviations between the mixing ratios of E-ZIF-7-*x* powders and XPS results, which may be attributed to the fact that XPS is a semi-quantitative analysis approach and the probed depth is only a few nanometers [37,38].

TEM imaging was carried out for all E-ZIF-7-*x* powders to observe the distribution of nanoparticles in organosilica networks. Fig. 7 (a–e) shows that nanoparticles were randomly distributed in the organosilica networks. The density of nanoparticles in the organosilica networks increased with doping content.

Due to the flexible properties of ZIF-7 structures, CO_2 could pass through the pores of nanoparticles [39]. Fig. 8 shows the CO_2 adsorption isotherms of BTESE, ZIF-7, and E-ZIF-7-0.4 powders measured at 25 ℃. The CO_2 adsorption uptakes decreased in the order of ZIF-7 > BTESE > E-ZIF-7-0.4. The CO_2 adsorption by E-ZIF-7-0.4 powders decreased dramatically, possibly due to the synergistic effect between ZIF-7 and BTESE, including the intrinsic pore size of ZIF-7 and the good compatibility between ZIF-7 and BTESE.

3.4. Gas separation performance

Fig. 9 (a) presents the gas permeance at 200 ℃ for BTESE and E-ZIF-7-*x* hybrid membranes. To compare the gas permeability of BTESE and E-ZIF-7-*x* hybrid membranes, the specific performances of the aforementioned membranes are depicted in Fig. 9 (b). The BTESE membrane has the highest gas permeances, while the H_2/CO_2 permselectivity of the BTESE membrane is only about 3 due to its loose structure. However, after incorporating nanoparticles into organosilica networks, the H_2 permeance of hybrid membranes decreased to ~1.0 × 10^{-6} mol·m^{-2}·s^{-1}·Pa^{-1}. Notably, the higher the doping content of ZIF-7 nanoparticles, the lower the permselectivity of hybrid membranes, indicating the appearance of non-selective channels for CO_2 permeation within the hybrid membranes. Interestingly, comparing E-ZIF-7-0.2 and E-ZIF-7-0.4 hybrid membranes, the H_2/CO_2 permselectivity slightly decreased, while the H_2 permeance increased to 1.2 × 10^{-6} mol·m^{-2}·s^{-1}·Pa^{-1}. In this study, the E-ZIF-7-0.4 hybrid membrane exhibited H_2 permeance of 1.2 × 10^{-6} mol·m^{-2}·s^{-1}·Pa^{-1} and H_2/CO_2 permselectivity of 21.7.

Fig. 10 illustrates the separation mechanism of hybrid membranes. The results show that incorporating ZIF-7 nanoparticles into BTESE networks provides not only additional gas permeation channels within the hybrid membranes but also molecular-sieving pores endowed by the intrinsic properties of nanoparticles, resulting in high H_2/CO_2 permselectivity. In contrast, when the doping content of ZIF-7 is excessive, nanoparticles tend to agglomerate in the BTESE networks to form non-selective pores, significantly decreasing the permselectivity of the hybrid membranes. Hence, the appropriate doping content of ZIF-7 nanoparticles enables hybrid membranes to have good gas separation performance.

The Normalized-Knudsen Permeance (NKP) method is used to measure the pore size of E-ZIF-7-*x* hybrid membranes, as shown in Fig. 11. The NKP equation is expressed using Eq. (4) [40,41]:

Table 4
H_2/CO_2 separation performance of membranes shown in Fig. 12[a].

Membranes	Temperature (℃)	Pressure (MPa)	Single gas/Mixed gas	H_2 permeance (mol·m^{-2}·s^{-1}·Pa^{-1})	H_2/CO_2 permselectivyty	References
PBI-PPA/CMS	150	0.65	Single-gas	5.0 × 10^{-7}	58	[42]
RUB-15	200	/	Single-gas	2.1 × 10^{-8}	105.6	[43]
$Zn_2(Bim)_4$	25	/	Mixed gas	3.7 × 10^{-7}	1084	[44]
NH_2-MIL-53/PMMA	25	0.2	Single-gas	3.3 × 10^{-8}	53.1	[45]
GO	25	0.1	Single-gas	1.9 × 10^{-6}	12.1	[46]
r-GO/BTESE	25	0.2	Single-gas	2.5 × 10^{-7}	4.1	[47]
POSi	200	0.69		1.2 × 10^{-7}	51	[48]
			Mixed gas	2.9 × 10^{-7}	36	
				3.1 × 10^{-7}	32	
E-ZIF-7-0.4	200	0.3	Single-gas	1.2 × 10^{-6}	21.7	This work

[a] The molar ratio of H_2 to CO_2 in the mixed gas is 1:1.

$$f_{NKP} = \frac{P_i}{P_{He}}\sqrt{\frac{M_i}{M_{He}}} = \frac{(d_p - d_{k,i})^3}{(d_p - d_{k,He})^3} \quad (4)$$

where d_p is the NKP pore size, P_i, P_{He} are the permeances of gas i and He, M_i and M_{He} are the molecular weight of gas i and He, $d_{k,i}$ and $d_{k,\,He}$ are the dynamic diameters of gas i and He, respectively.

Fig. 11 shows the NKP plot as a function of molecule size of E-ZIF-7-x hybrid membranes. From the fitting lines, the calculated pore size of the E-ZIF-7-x hybrid membranes increased from 0.398 to 0.504 nm. The agglomeration of nanoparticles in the organosilica networks may cause an increase in the pore size of the hybrid membranes. The above results indicated that the doping content of nanoparticles might significantly influence the pore size of organosilica membranes.

Fig. 12 compares the H_2/CO_2 separation performance of MOF/organosilica hybrid materials with previous membranes, such as carbon membrane [42], molecular sieve membrane [43], MOF-doped mixed matrix membranes [44,45], GO-based membranes [46,47], and POSi membranes [48]. Based on Fig. 12, MOF/organosilica hybrid membranes have good H_2/CO_2 separation performance, far beyond the 2008 upper bound. Table 4 summarizes the H_2/CO_2 separation performance of membranes shown in Fig. 12.

4. Conclusion

A series of MOF/organosilica hybrid membranes were successfully prepared. The XRD, FTIR, XPS, and TEM characterizations confirmed that nanoparticles had been introduced into organosilica networks. The effect of ZIF-7 doping content on the separation performance and the related separation mechanisms of E-ZIF-7-x hybrid membranes were investigated. Neither low nor high doping content of ZIF-7 nanoparticles could achieve the expected H_2/CO_2 permselectivity. When the doping content was suitable, the corresponding hybrid membranes could take full advantage of ZIF-7 nanoparticles to obtain improved separation performance. The E-ZIF-7-0.4 membrane exhibited improved H_2/CO_2 permselectivity with high H_2 permeance. The organosilica membranes with appropriate ZIF-7 doping content were suitable for pre-combustion capture.

CRediT authorship contribution statement

Yi Ren: Conceptualization, Methodology, Formal analysis, Investigation, Visualization, Data curation, Validation, Writing – original draft. **Die He:** Formal analysis, Investigation, Visualization. **Tong Wang:** Formal analysis, Investigation, Visualization. **Hong Qi:** Resources, Validation, Writing – review & editing, Funding acquisition, Project administration, Supervision.

Declaration of Competing Interest

The authors declare that they have no known competing financial interests or personal relationships that could have appeared to influence the work reported in this paper.

Data availability

Data will be made available on request.

Acknowledgments

The National Natural Science Foundation of China (21490581) and China Petroleum & Chemical Corporation (317008-6) supported this study.

References

[1] T. Wilberforce, A.G. Olabi, E.T. Sayed, K. Elsaid, M.A. Abdelkareem, Progress in carbon capture technologies, Sci. Total Environ. 761 (2021), 143203.
[2] A. Midilli, M. Ay, I. Dincer, M.A. Rosen, On hydrogen and hydrogen energy strategies I: current status and needs, Renew. Sustain. Energy Rev. 9 (2005) 255–271.
[3] C. Tarhan, M.A. Çil, A study on hydrogen, the clean energy of the future: Hydrogen storage methods, J. Energy Storage. 40 (2021), 102676.
[4] X. Hu, J. Huang, X. He, Q. Luo, C. Li, C. Zhou, R. Zhang, Analyzing the potential benefits of trio-amine systems for enhancing the CO_2 desorption processes, Fuel. 316 (2022), 123216.
[5] A.M. Yousef, W.M. El-Maghlany, Y.A. Eldrainy, A. Attia, New approach for biogas purification using cryogenic separation and distillation process for CO_2 capture, Energy. 156 (2018) 328–351.
[6] N. Norahim, P. Yaisanga, K. Faungnawakij, T. Charinpanitkul, C. Klaysom, Recent membrane developments for CO_2 separation and capture, Chem. Eng. Technol. 41 (2018) 211–223.
[7] W. Yong, H. Zhang, Recent advances in polymer blend membranes for gas separation and pervaporation, Prog. Mater. Sci. 116 (2021), 100713.
[8] W. Wang, G. Olguin, D. Hotza, M.A. Seelro, W. Fu, Y. Gao, G. Ji, Inorganic membranes for in-situ separation of hydrogen and enhancement of hydrogen production from thermochemical reactions, Renew. Sustain. Energy Rev. 160 (2022), 112124.
[9] C. Chuah, X. Jiang, K. Goh, R. Wang, Recent progress in mixed-matrix membranes for hydrogen separation, Membranes. 11 (2021) 666.
[10] N. Moriyama, M. Ike, H. Nagasawa, M. Kanezashi, T. Tsuru, Network tailoring of organosilica membranes via aluminum doping to improve the humid-gas separation performance, RSC Adv. 12 (2022) 5834–5846.
[11] M.C. Duke, J.C.D. da Costa, D.D. Do, P.G. Gray, G.Q. Lu, Hydrothermally robust molecular sieve silica for wet gas separation, Adv. Funct. Mater. 16 (2006) 1215–1220.
[12] M. Kanezashi, K. Yada, T. Yoshioka, T. Tsuru, Design of silica networks for development of highly permeable hydrogen separation membranes with hydrothermal stability, J. Am. Chem. Soc. 131 (2009) 414–415.
[13] K. Chang, T. Yoshioka, M. Kanezashi, T. Tsuru, K. Tung, A molecular dynamics simulation of a homogeneous organic–inorganic hybrid silica membrane, Chem. Commun. 46 (2010) 9140.
[14] H. Zhang, D. He, S. Niu, H. Qi, Tuning the microstructure of organosilica membranes with improved gas permselectivity via the co-polymerization of 1,2-bis (triethoxysilyl)ethane and 1,2-bis(triethoxysilyl)methane, Int. J. Hydrogen Energy. 46 (2021) 17221–17230.
[15] S. Chai, H. Du, Y. Zhao, Y. Lin, C. Kong, L. Chen, Fabrication of highly selective organosilica membrane for gas separation by mixing bis(triethoxysilyl)ethane with methyltriethoxysilane, Sep. Purif. Technol. 222 (2019) 162–167.
[16] J. Li, D.K. Wang, H. Tseng, M. Wey, Solvent effects on diffusion channel construction of organosilica membrane with excellent CO_2 separation properties, J. Membr. Sci. 618 (2021), 118758.
[17] N. Moriyama, H. Nagasawa, M. Kanezashi, K. Ito, T. Tsuru, Bis(triethoxysilyl) ethane (BTESE)-derived silica membranes: pore formation mechanism and gas permeation properties, J. Sol-Gel Sci. Technol. 86 (2018) 63–72.
[18] H. Song, Y. Wei, H. Qi, Tailoring pore structures to improve the permselectivity of organosilica membranes by tuning calcination parameters, J. Mater. Chem. A 5 (2017) 24657–24666.
[19] H. Zhang, Y. Wei, S. Niu, H. Qi, Fabrication of Pd-Nb bimetallic doped organosilica membranes by different metal doping routes for H_2/CO_2 separation, Chin. J. Chem. Eng. 36 (2021) 67–75.
[20] D. He, H. Zhang, Y. Ren, H. Qi, Fabrication of a novel microporous membrane based on ZIF-7 doped 1,2-bis(triethoxysilyl)ethane for H_2/CO_2 separation, Microporous Mesoporous Mater. 331 (2022), 111674.
[21] Q. Qian, P.A. Asinger, M.J. Lee, G. Han, K. Mizrahi Rodriguez, S. Lin, F. M. Benedetti, A.X. Wu, W.S. Chi, Z.P. Smith, MOF-based membranes for gas separations, Chem. Rev. 120 (2020) 8161–8266.
[22] L. Xiang, L. Sheng, C. Wang, L. Zhang, Y. Pan, Y. Li, Amino-functionalized ZIF-7 nanocrystals: improved intrinsic separation ability and interfacial compatibility in mixed-matrix membranes for CO_2/CH_4 separation, Adv. Mater. 29 (2017) 1606999.
[23] M. Shah, M.C. McCarthy, S. Sachdeva, A.K. Lee, H. Jeong, Current status of metal-organic framework membranes for gas separations: promises and challenges, Ind. Eng. Chem. Res. 51 (2012) 2179–2199.
[24] M.R. Abdul Hamid, T.C. Shean Yaw, M.Z. Mohd Tohir, W.A. Wan Abdul Karim Ghani, P.D. Sutrisna, H. Jeong, Zeolitic imidazolate framework membranes for gas separations: current state-of-the-art, challenges, and opportunities, J. Ind. Eng. Chem. 98 (2021) 17–41.
[25] S. Shafiq, B.A. Al-Maythalony, M. Usman, M.S. Ba-Shammakh, A.A. Al-Shammari, ZIF-95 as a filler for enhanced gas separation performance of polysulfone membrane, RSC Adv. 11 (2021) 34319–34328.
[26] Y. Wang, Y. Ren, H. Wu, X. Wu, H. Yang, L. Yang, X. Wang, Y. Wu, Y. Liu, Z. Jiang, Amino-functionalized ZIF-7 embedded polymers of intrinsic microporosity membrane with enhanced selectivity for biogas upgrading, J. Membr. Sci. 602 (2020), 117970.
[27] S. Yang, Y. Wang, P. Lu, H. Jin, F. Pan, Z. Shi, X. Jiang, C. Chen, Z. Jiang, Y. Li, Metal-organic frameworks corset with a thermosetting polymer for improved molecular-sieving property of mixed-matrix membranes, ACS Appl. Mater. Interfaces 12 (2020) 55308–55315.

[28] S. Yoon, H. Lee, S. Hong, CO_2/N_2 gas separation using Pebax/ZIF-7-PSf composite membranes, Membranes 11 (2021) 708.
[29] C. Kong, H. Du, L. Chen, B. Chen, Nanoscale MOF/organosilica membranes on tubular ceramic substrates for highly selective gas separation, Energy Environ. Sci. 10 (2017) 1812–1819.
[30] Y. Li, F. Liang, H. Bux, A. Feldhoff, W. Yang, J. Caro, Molecular sieve membrane: supported metal-organic framework with high hydrogen selectivity, Angew. Chem. Int. Ed. 49 (2010) 548–551.
[31] R. Al-Oweini, H. El-Rassy, Synthesis and characterization by FTIR spectroscopy of silica aerogels prepared using several $Si(OR)_4$ and $R''Si(OR')_3$ precursors, J. Mol. Struct. 919 (2009) 140–145.
[32] P.H. Tchoua Ngamou, J.P. Overbeek, R. Kreiter, V.H.M. Veen, J.F. Vente, I. M. Wienk, P.F. Cuperus, M. Creatore, Plasma-deposited hybrid silica membranes with a controlled retention of organic bridges, J. Mater. Chem. A. 1 (2013) 5567–5576.
[33] C. Kang, Y. Lin, Y. Huang, K. Tung, K. Chang, J. Chen, W. Hung, K. Lee, J. Lai, Synthesis of ZIF-7/chitosan mixed-matrix membranes with improved separation performance of water/ethanol mixtures, J. Membr. Sci. 438 (2013) 105–111.
[34] Y. Ying, Y. Xiao, J. Ma, X. Guo, H. Huang, Q. Yang, D. Liu, C. Zhong, Recovery of acetone from aqueous solution by ZIF-7/PDMS mixed matrix membranes, RSC Adv 5 (2015) 28394–28400.
[35] H. Song, S. Zhao, J. Lei, C. Wang, H. Qi, Pd-doped organosilica membrane with enhanced gas permeability and hydrothermal stability for gas separation, J. Membr. Sci. 51 (2016) 6275–6286.
[36] J. Gao, H. Mao, H. Jin, C. Chen, A. Feldhoff, Y. Li, Functionalized ZIF-7/Pebax® 2533 mixed matrix membranes for CO_2/N_2 separation, Microporous Mesoporous Mater. 297 (2020), 110030.
[37] A.G. Shard, Practical guides for x-ray photoelectron spectroscopy: Quantitative XPS, J. Vac. Sci. Technol. A 38 (2020) 41201.
[38] B. Robert, V. Flaud, R. Escalier, A. Mehdi, C. Vigreux, XPS study of Ge–Se–Te surfaces functionalized with organosilanes, Appl. Surf. Sci 607 (2023), 154921.
[39] A. Noguera Díaz, J. Villarroel Rocha, V.P. Ting, N. Bimbo, K. Sapag, T.J. Mays, Flexible ZIFs: probing guest-induced flexibility with CO_2, N_2 and Ar adsorption, J. Chem. Technol. Biotechnol. 94 (2019) 3787–3792.
[40] R. Xu, Q. Liu, X. Ren, P. Lin, J. Zhong, Tuning the pore structures of organosilica membranes for enhanced desalination performance via the control of calcination temperatures, Membranes 10 (2020) 392.
[41] L. Meng, M. Kanezashi, J. Wang, T. Tsuru, Permeation properties of BTESE–TEOS organosilica membranes and application to O_2/SO_2 gas separation, J. Membr. Sci. 496 (2015) 211–218.
[42] L. Hu, V.T. Bui, A. Krishnamurthy, S. Fan, W. Guo, S. Pal, X. Chen, G. Zhang, Y. Ding, R.P. Singh, M. Lupion, H. Lin, Tailoring sub – 3.3 Å ultramicropores in advanced carbon molecular sieve membranes for blue hydrogen production, Sci. Adv. 8 (2022), l8160.
[43] M. Dakhchoune, L.F. Villalobos, R. Semino, L. Liu, M. Rezaei, P. Schouwink, C. E. Avalos, P. Baade, V. Wood, Y. Han, M. Ceriotti, K.V. Agrawal, Gas-sieving zeolitic membranes fabricated by condensation of precursor nanosheets, Nat. Mater. 20 (2021) 362–369.
[44] L. Shu, Y. Peng, R. Yao, H. Song, C. Zhu, W. Yang, Flexible soft-solid metal-organic framework composite membranes for H_2/CO_2 separation, Angew. Chem. Int. Ed. 61 (2022) e202117577.
[45] Y. Zhao, D. Zhao, C. Kong, F. Zhou, T. Jiang, L. Chen, Design of thin and tubular MOFs-polymer mixed matrix membranes for highly selective separation of H_2 and CO_2, Sep Purif. Technol. 220 (2019) 197–205.
[46] J.P. Kim, E. Choi, J. Kang, S.E. Choi, Y. Choi, O. Kwon, D.W. Kim, Ultrafast H_2-selective nanoporous multilayer graphene membrane prepared by confined thermal annealing, Chem. Commun. 57 (2021) 8730–8733.
[47] Y. Zhao, C. Zhou, C. Kong, L. Chen, Ultrathin reduced graphene oxide/organosilica hybrid membrane for gas separation, JACS Au 1 (2021) 328–335.
[48] L. Zhu, L. Huang, S.R. Venna, A.K. Blevins, Y. Ding, D.P. Hopkinson, M.T. Swihart, H. Lin, Scalable polymeric few-nanometer organosilica membranes with hydrothermal stability for selective hydrogen separation, ACS Nano 15 (2021) 12119–12128.